

## EFFECTS OF CONCRETE SLAB ON DUCTILITY OF STEEL MOMENT CONNECTIONS

Changbin Joh<sup>1</sup> and Wai-Fah Chen<sup>2</sup>

<sup>1</sup> Korea Institute of Construction Technology (KICT), 2311 Daehwa-Dong, Ilsan-Gu, Goyang-Si,  
Gyeonggi-Do, 411-712 Korea.

Tel: 82-31-9100-332 Fax: 82-31-9100-121 Email: cjoh@kict.re.kr

<sup>2</sup> College of Engineering, University of Hawaii at Manoa 2540 Dole Street, Holmes Hall 240,  
Honolulu, HI 96822, USA.

Tel: (808)956-7727 Fax: (808)956-2291 Email: chenwf@wiliki.eng.hawaii.edu

**Abstract:** The effects of slab on the ductility of steel moment connections representing typical Japanese and US details are investigated based on an interpretation of existing composite connection tests and our own numerical analyses. Different seismic behaviors between typical Japanese and US connections are also investigated. The results show that the presence of slab: increases the beam strength, imposes a constraint near the beam top flange, and, as a consequence, induces concentrated deformation near the beam bottom flange, which in turn reduces the ductility of the connection. The total deformation capacity of the connection depends not only on the beam but also on the connecting column and panel zone. The detrimental slab effects and the relative strength between beams, column, and panel zone should be considered in the seismic design of these connections.

**Keywords:** Seismic Design, Concrete Slab, Local Ductility, Steel Moment Connection, Rupture Index, Relative Strength

### 1. INTRODUCTION

During the Northridge in 1994 and Hyogoken-Nanbu in 1995 earthquakes, Steel Moment Connections (SMC) failed in a brittle manner. These connections were designed to have a ductile and stable failure mechanism such as the formation of a plastic hinge. Most of the brittle failure occurred at the column weld interface of the lower portion of the connection (Figure 1). These unexpected failures initiated several experimental studies on SMCs with various reinforcements and improved details. The improvements include the use of Reduced Beam Section (RBS), haunches, and cover plate (FEMA [1] and Nakashima et al., [2]) both in Japan and US. These studies focused on the tests of full-scale sub-assemblages of a column and a beam to guarantee energy dissipation through the stable formation of a plastic hinge at the beam.

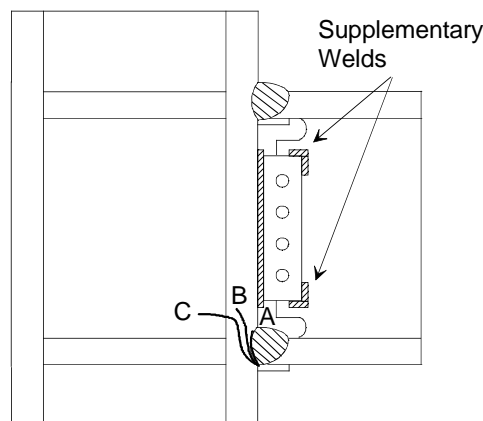


**Figure 1.** Typical Damages During Northridge Earthquake (Joh and Chen 1999)

Most of these test specimens, however, did not consider the composite action of the slab. This is probably because of the assumption that the composite connection will behave like a bare steel connection after a few cycles of earthquake loading due to the cracks at the face of a column flange.

Since an actual steel building frame has floor slabs that are bonded to supporting beams from full to partial composite actions, its actual behavior under earthquake load will be different from what is expected from a bare steel building. For instance, the composite connection will attract more moment than that from the analysis based on the bare steel building. On the other hand, under the same story drift, a composite connection needs more local deformation capacity than a bare steel connection. The reason is that the composite slab adds constraint to the top of the connection, concentrates the deformation at the lower portion of the connection, and eventually reduces the global deformation capacity. In spite of some of these cracks at the face of the column flange, the composite action might be quite effective as will be shown later.

Another relatively less studied issue is the relative strength effect on the seismic behavior of the SMC. Total deformation of the SMC is the sum of the deformation from beams, columns, and panel zone. Contribution of each component is dependent on the relative strength between the connection components; the columns, the beams, and the panel zone. Due to the strong column-weak beam design concept, the ductility of a SMC largely depends on the deformation capacity of the beam. However, with a relatively less strong column, the burden of a beam can be lowered without lowering the total ductility of a SMC.

In this paper, the slab effects on the deformation capacity of a SMC are investigated using the interpretation and numerical analyses of composite connection tests. The untested connection details are also numerically analyzed based on our successful numerical modeling of the tested specimens. The relative strength effects are also investigated based on the numerical analysis. The contribution to the total deformation from each connection component is quantified and compared between typical Japanese and US connections.

## **2. STEEL MOMENT CONNECTION IN USA AND JAPAN**

Seismic design codes require that structural integrity be maintained under site-specific earthquake excitations. To achieve this, steel moment connections are designed to attain the plastic moment ( $M_p$ ) in the beams and the columns without allowing the fracture of the connection itself. Moreover, the "strong column-weak beam" concept is often used to force the formation of plastic hinges in the beams to minimize lateral deflections and global stability. This design concept is taken for granted in two high seismic regions in the world: Japan and USA.

However, typical details of the connections between Japan and US practices are different each other, because design practice are closely related with not only the design concept but also with the material and the fabrication skills used in the region. In this section, typical connection details for Japan and USA are briefly reviewed and the composite connection tests used in this paper will then be described.

## 2.1 USA: before and after the Northridge Earthquake

The welded flange-bolted web (WFBW) connection uses the principle and design details as shown in Figure 1. The column is continuous through the joint. Shear plates are welded to the column flange in the shop and bolted to the beam web in the field. Beam flanges are welded to column flanges using full penetration butt groove welding. An E70T-4, the self-shielded flux cored electrode with a very low toughness, was commonly used. During the Northridge earthquake, while the top flange of beams and shear tabs showed some damage, brittle failures at the column-weld interface were most common (Figure 1, Joh and Chen, [3]).

After the Northridge earthquake, SAC Joint Venture initiated several projects to investigate the connection failures experimentally and analytically (FEMA, [1]). These test results lead to two conclusions. First, the standard WFBW connection demonstrated poor performance (brittle fracture). Second, reinforced connections with reduced beam sections (RBS, Figure 2(a)) and haunches (Figure 2(b)) can improve the performance of standard moment connections. It should be noted that most of these test setups did not include the composite floor slab.

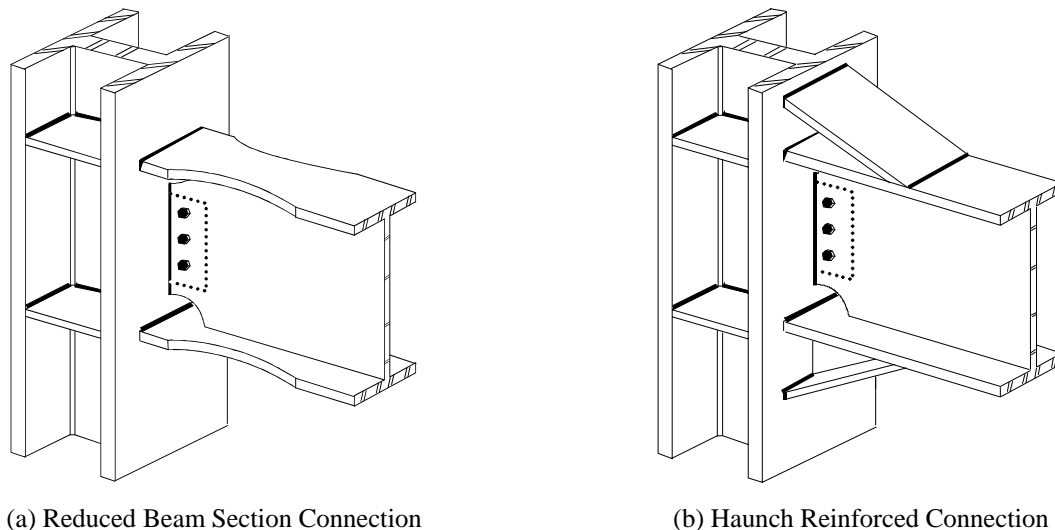


**Figure 2.** Improved Connection Details after Northridge Earthquake

## 2.2 Japan: before and after the Hyogoken-Nanbu Earthquakes

In Japan, modern steel moment frames are usually constructed using square tube column (often cold-formed) and wide flange beams known as a ‘through-diaphragm connection’ (Nakashima et al., [2]). In this connection, a square tube is cut into three pieces, one for the panel zone, others for the lower and upper columns respectively (Figure 3). Two diaphragm plates slightly bigger than the square tube are placed between the columns and shop welded all around by full penetration groove welding. A short segment of wide flange section is then welded to the diaphragm in the shop using full penetration groove welding to guarantee high quality welding at the stress concentrated region. Then the beam web is fillet welded to the column. Later in the field, mid-span of the beam is connected by the bolted splice. This type of connection is very popular in Japan, particularly for low and mid-rise buildings.

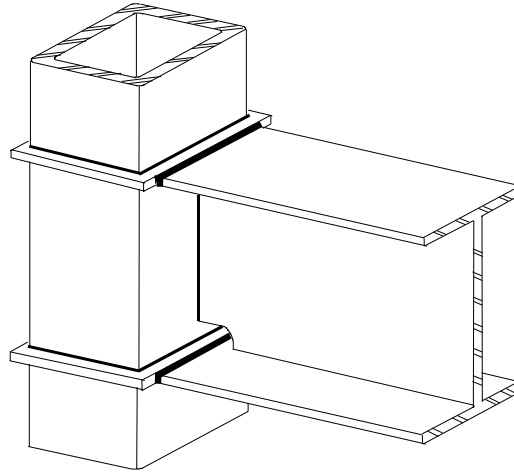


**Figure 3.** Typical Japanese Connection

After the Hyogoken-Nanbu earthquake, many damages were found in this connection. Most of these failures are, with some degree of plastic deformation and local buckling in the beam, brittle fracture at the weld metal or beam base metal near weld toe (Nakashima et al., [2]). Possible causes are: stress concentrated at the web access hole with low fracture toughness, concentrated welding near the beam flange due to a short diaphragm, and an un-removed backing bar.

### 3. COMPOSITE CONNECTION TESTS

#### 3.1 Composite Connection Test: Japanese Connections

For the composite connection tests representing Japanese connection detailing, the tests performed at the Research Institute of Industrial Science and Technology (RIST) are used. (RIST, [4], and Joh and Chen, [5]). Of 10 specimens tested with many parameters, 3 specimens representing composite steel connections (S01 and S04) and a bare steel connection (S02) are numerically modeled to investigate the slab effects (Table 1).

**Table 1.** Details of Japanese Connections

| <b>Model<br/>(1)</b> | <b>Column<br/>(2)</b> | <b>Beam<br/>(3)</b>   | <b>Slab<br/>(4)</b> | <b>Comment<br/>(5)</b> |
|----------------------|-----------------------|-----------------------|---------------------|------------------------|
| S01                  | B-Box-450 x 450 x 22  | H-612 x 202 x 13x 23  | 200 mm              | Standard Slab          |
| S02                  | B-Box-450 x 450 x 22  | H-612 x 202 x 13 x 23 | - -                 | No Slab, Bare Steel    |
| S04                  | B-Box-450 x 450x 22   | H-612 x 202 x 13 x 23 | 130 mm              | Shallow Slab           |

The test specimen is designed to represent the lower part of a moment connection of typical 10-story building in Japan. The column height between the hinges is 3.7 m and the beam length from the face of the column is 3.275 m (Figure 4). For columns, the square box sections (B-Box-450 x 450 x 22) with the height and the width of 450 mm and the thickness of 22 mm are used. For beams, H sections (H-612 x 202 x 13 x 23) with the height of 612 mm and the width of 202 mm are used. The thickness of the web and the flange are 13 mm and 23 mm respectively. Real scale top and bottom box columns are welded each other using a 25 mm thick complete penetration diaphragm. Beam flanges (23 mm thick) are welded to this diaphragm instead of a column flange and beam access hole is used as shown in Figure 4. The beam web is welded to a column flange directly without using a shear tab. To see the slab effects clearly, the panel zone is designed to

remain elastic range even under ultimate loading. To simulate the actual steel building, four side beams are designed at each column web and each side of loading zone, and fully bonded to the slab using 22 mm diameter stud bolts. To have complete composite action between the beam and slab, two 22 mm diameter studs are used at 200 mm spacing. All steel materials used are SM490 and their material properties are shown in Table 2.

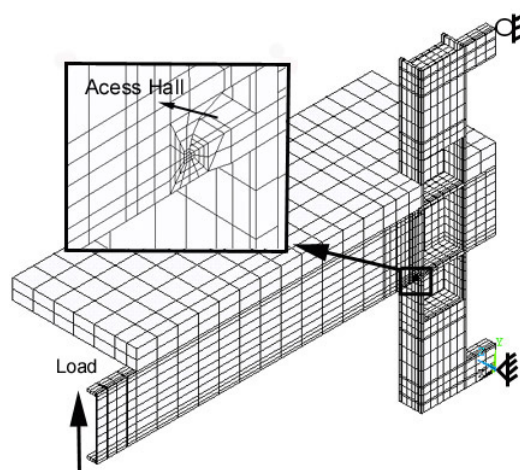


**Figure 4.** Numerical Model for a Japanese Connection (S01)

**Table 2.** Material Properties of Japanese Connections

| Specimen<br>(1) | $\sigma_y$ (MPa)<br>(2) | $\sigma_u$ (MPa)<br>(3) | $\sigma_y / \sigma_u$<br>(4) | Elongation (%)<br>(5) |
|-----------------|-------------------------|-------------------------|------------------------------|-----------------------|
| Plate           | 374.4                   | 541.9                   | 0.59                         | 24.5                  |
| Flange          | 390.4                   | 536.1                   | 0.65                         | 25.5                  |
| Web             | 443.9                   | 551.7                   | 0.81                         | 24.9                  |

Concrete slab is designed to represent thick and thin slabs. Concrete strength measured at the time of the test is 25.7 MPa. For reinforcement, both 30 mm from the top and bottom of the slab, D13 (diameter = 13 mm) bar at 200 mm spacing in both directions are used. The members of the specimens numerically modeled are described in Table 2. The major difference between composite specimens (S01 and S04) is the thickness of slab and other details are identical to S01.

The failure of S01 specimen occurred at the root of bottom flange access hole, which is similar to the damage occurred during the Hyogoken-Nanbu earthquake (RIST, [4], and Joh and Chen, [5]). Under cyclic loading, semi-elliptic ductile crack is propagated from the root of bottom flange access hole, where the geometry changes abruptly and crack-like defects can be found due to the cutting process of access hole. After this ductile crack reaches its critical size, the brittle fracture occurs.

Figures 5 and 6 show the test results of global behavior of S01 and S02. The displacement in the figures is the displacement measured at the loading position (here after 'Beam Tip Displacement'). Due to the composite action of the slab, S01 has greater strength than that of S02. For the ductility of the connection, however, S02, a bare steel connection, took more cyclic loading before it failed than S01 did. Therefore, S01 has smaller deformation and energy dissipation capacity than that of S02. This is because the slab increases the constraint near the top flange and deformation is concentrated at the lower flange as shown in the numerical analysis. The specimen, S04, with a

shallower slab, has smaller ultimate strength than that of S01 but shows similar deformation behavior to S01. More test results will be discussed along with numerical analysis later.

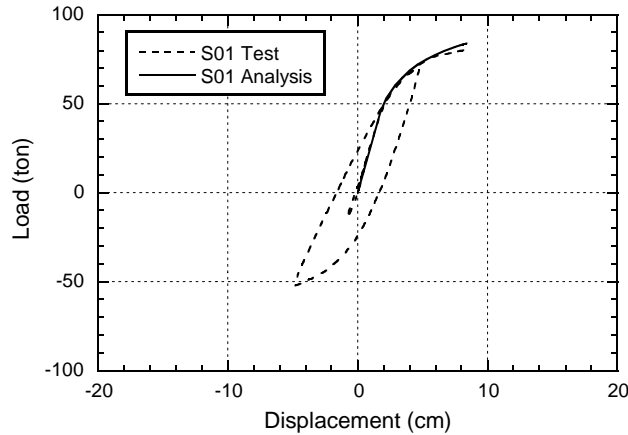


**Figure 5.** Global Behavior of a Japanese Connection (S01, Composite Connection)

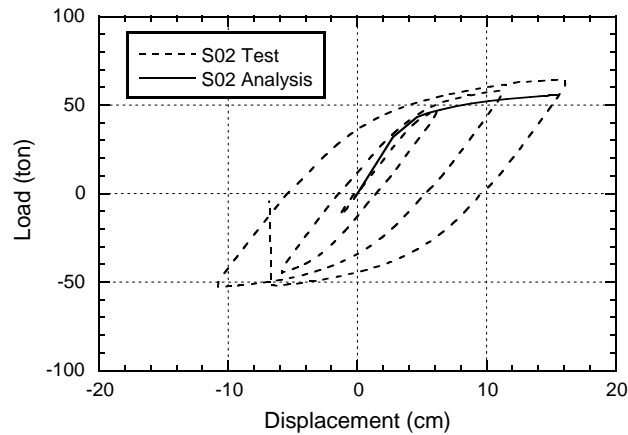


**Figure 6.** Global Behavior of a Japanese Connection (S02, Bare Steel Connection)

### 3.2 Numerical Model

Numerical models are used to investigate the local behavior near the beam access hole, where the fracture occurs, not for the detailed behavior of the slab. Figure 4 shows the numerical model of a composite connection (S01). Only one-half is modeled due to the symmetry. 8-node solid elements are used for a bare steel connection and concrete slab using ANSYS commercial code (ANSYS, [6]). For the local behavior near stress concentration, the meshes in the vicinity of the access hole are finer than the meshes for other region (Figure 4). Hinged boundary conditions are imposed at both ends of the column to describe the test setup. Monotonously increasing load is applied at the end of the beam. Multi-linear isotropic hardening model is used for the steel beam and the column based on the material test results (Table 2). Concrete slab is modeled as the Drucker-Prager material, because our primary concern of the analysis is not the detailed behavior of the slab such as cracking but the behavior near the beam access hole.

In the composite specimens (S01 and S04), constraint equations are used to connect the slab to the steel beam and column, which has achieved full composite action (i.e., no slip). Side beams are also simulated by the constraint equation. Reinforcing bars in the slab are not modeled for simplicity.

### 3.3 Composite Connection Test: US Connections

The tests performed by Civjan et al. are modeled (Civjan et al., [7,8]). The original purpose of the test was to find an effective and economic repair method for existing connections. Four specimens representing composite steel connections (DB2 and HCH4) and bare steel connections (DB1 and HCH3) are numerically modeled to investigate the effects of the slab (Table 3). DB1 and DB2 are RBS connections, and HCH3 and HCH4 are reinforced with haunches. DB1 and HCH3 are identical to DB2 and HCH4 respectively except the presence of the slab.

**Table 3.** Details of US Connections

| Model<br>(1) | Column<br>(2) | Beam<br>(3) | Slab<br>(4) | Comment<br>(5)       |
|--------------|---------------|-------------|-------------|----------------------|
| DB1          | W12 x 279     | W30 x 99    | No Slab     | Bottom flange<br>RBS |
| DB2          | W12 x 279     | W30 x 99    | 160 mm      | Bottom flange<br>RBS |
| HCH3         | W12 x 279     | W30 x 99    | No Slab     | Bottom haunch        |
| HCH4         | W12 x 279     | W30 x 99    | 160 mm      | Bottom haunch        |

Figures 7 and 8 show the connection test setup schematically for DB 2 and HCH4 respectively. The column height between the hinge at the bottom and the loading is 3.66 m and the beam length between the hinges is 7.32 m (Figure 7 and 8). Actually, both ends of the beams are supported by rigid-link with load cell from the floor. In the test, specimens were loaded at the top of the column under quasi-static cyclic loading as per ATC-24 (ATC-24, 1992) guidelines. The test specimens are designed to represent retrofitted connections from typical mid-1970s pre-Northridge building. RBS retrofitting is only applied to the beam bottom flange considering the high cost and practical difficulty of applying RBS to the upper flange in the presence of slab. The haunch retrofitting is applied to weld wide flange section into the area of intersection of the lower beam flange and the column flange for the same reason. For the column, W12 x 279 (Gr. 50) and, for the beam, W30 x 99 (A36) are used for all specimens. For HCH3 and HCH4, haunches are cut from W21 x 139 (Gr. 50). Material properties are shown in Table 4.

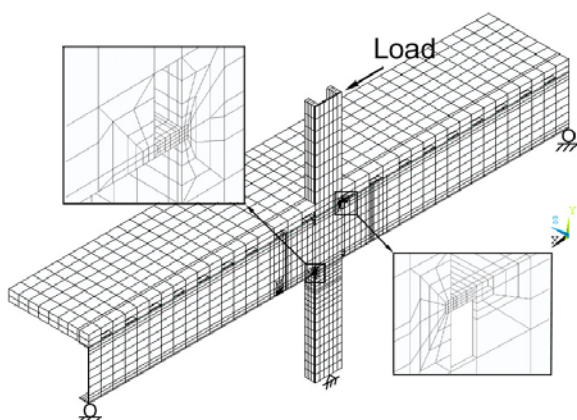


**Figure 7.** Numerical Model for an US Connection (DB2)

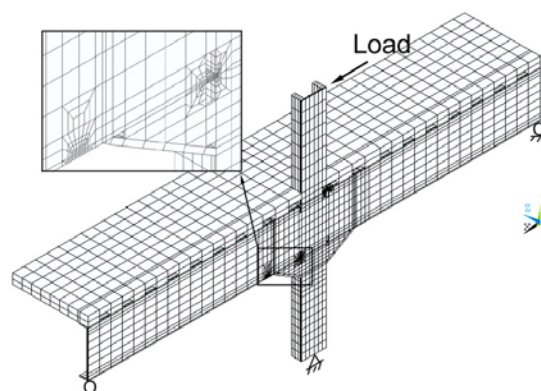


**Figure 8.** Numerical Model for an US Connection (HCH4)

**Table 4.** Material Properties of US Connections

| Specimen<br>(1)     | Static $\sigma_y$ (MPa)<br>(2) | Dyn. $\sigma_y$ (MPa)<br>(3) | Dyn. $\sigma_u$ (MPa)<br>(4) | $\sigma_y/\sigma_u$<br>(5) |
|---------------------|--------------------------------|------------------------------|------------------------------|----------------------------|
| Beam                | 329                            | 345                          | 452                          | 0.76                       |
| Column <sup>a</sup> | 379 (assumed)                  | - -                          | 521.4 (assumed)              | - -                        |

<sup>a</sup>A572 Gr. 50 is used for columns but no specific data are not available from the reference (Civjan et al., [7,8]). For numerical modeling, typical material properties for A572 Gr. 50 are used.

For the slab, lightweight concrete was used with metal decking oriented perpendicular to the beam. To represent the partial composite action of existing buildings, location and number of studs are decided and the rate of composite action as defined by the AISC LRFD specification is approximately 18%. Concrete strengths measured at the time of the test were 33.7 MPa and 22.2 MPa for DB2 and HCH4 respectively. For reinforcement, No 3 bars were placed perpendicular to the beam preventing temperature and shrinkage cracking and for longitudinal reinforcement, 6 x 6 wire meshes were used.

The test results show that simply applying RBS to the beam bottom flange alone to the pre-Northridge connection will not improve its seismic performance, but haunch reinforcing would be an effective way to retrofit the old connections.

Figures 9, 10, 11 and 12 show the envelope curves of hysteresis curves of these tested specimens. The envelope curve is the curve connecting the peak response points of the first cycle in the second quadrant for each of deformation amplitude. The displacement in the figures is the displacement measured at the loading position (here after 'Column Tip Displacement'). Due to the composite action of the slab, DB2 has greater strength than that of DB1. However, DB2 has greater deformation and energy dissipation capacity than that of DB1, which is just opposite from what is observed in the Japanese connection test. Similar results can be observed from those of HCH3 and HCH4. DB2. The composite RBS connection achieved the plastic rotation of 0.02, while DB1, the bare steel connection, only achieved the plastic rotation in the range of 0.006 - 0.009. The haunch reinforced specimen, HCH4, achieved the plastic rotation in the range of 0.028 - 0.055, while HCH3 achieved the plastic rotation in the range of 0.012-0.023.

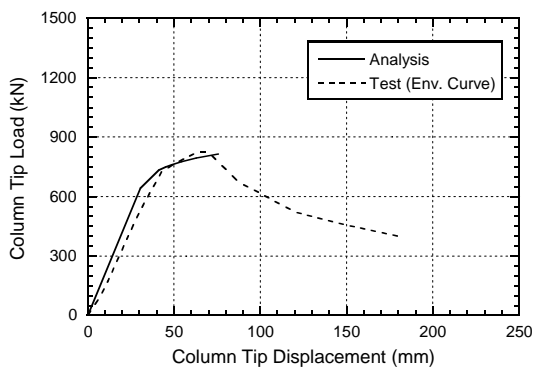


**Figure 9.** Global Behavior of an US Connection (DB1, Bare Steel Connection)

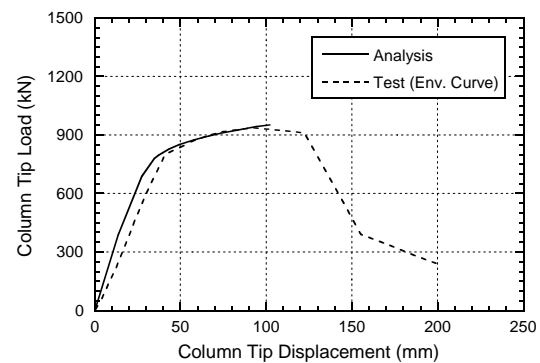


**Figure 10.** Global Behavior of an US Connection (DB2, Composite Connection)

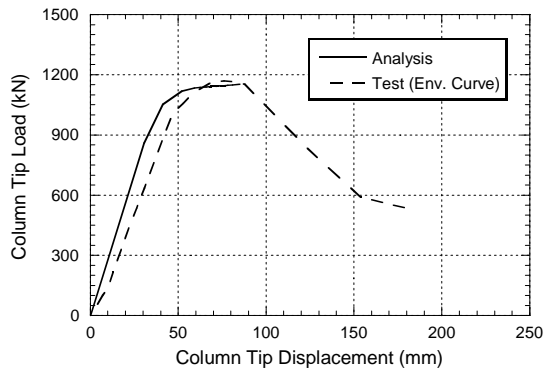


**Figure 11.** Global Behavior of an US Connection (HCH3, Bare Steel Connection)

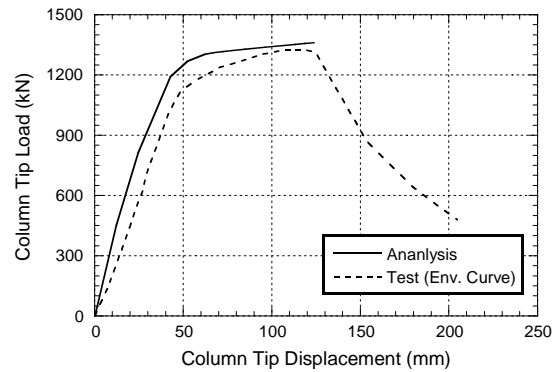


**Figure 12.** Global Behavior of an US Connection (HCH4, Composite Connection)

According to this result, the presence of the slab does improve the ductility of the connection, and the concentration of the beam deformation due to the confining effect of the slab does not occur. This beneficial effect of the slab comes from the lateral support and the delaying of local buckling due to the presence of the slab. In fact, according to the references (Civjan et al., [7,8]), the bare steel connections showed some lateral instabilities during the loading stage, probably due to the poor test setup. Nevertheless, since no actual building has bare steel frame alone, this effect is taken for granted. The possible explanation why the detrimental effect of the slab was not seen for the connection with the US detailing will be discussed in the next section. Detailed information about these test results can be found in the references (Civjan et al., [7,8]).

### 3.4 Numerical Model

Figures 7 and 8 also show numerical models to investigate the local behavior near stress concentrated area. As before, only one-half is modeled due to the symmetry. 8-node solid elements are used for the bare steel connection and concrete slab using ANSYS commercial code (ANSYS, [6]). For the local behavior of the RBS specimens, the meshes near the beam flanges in tension are finer than the meshes for other region (Figures 7 and 8). In Figure 7, the RBS is modeled at the beam bottom flange, although modeling is not shown due to the viewing direction. For the haunch reinforced model, additional fine meshes are applied in front of the haunch where the local buckling occurred during the test. Hinged boundary conditions are imposed at both ends of the beam to simulate test setup. Monotonously increasing load is applied at the end of the column. Again, multi-linear isotropic hardening model is used for the steel beam and the column based on the material properties reported (Table 4).

Flute concrete slab is modeled, but metal decking is not modeled because the metal decking is considered as a secondary member. For the composite specimens (DB2 and HCH4), constraint equations are used again to connect the slab to the steel beam and column to achieve a partial composite action (i.e., slip). No reinforcing bars are modeled.

## 4. NUMERICAL RESULTS AND DISCUSSION

### 4.1 Rupture Index

To evaluate and compare fracture potential relatively between different connection models, a rupture index (RI) is computed at the reported critical location from the tests. The definition of RI is as follows,

$$RI = \frac{\varepsilon_{ep} / \varepsilon_y}{\exp(-1.5\sigma_h / \sigma_{mises})} \quad (1)$$

where,  $\varepsilon_{ep}$  is effective plastic strain ( $(2\varepsilon_{ij}^p \varepsilon_{ij}^p / 3)^{0.5}$ ),  $\varepsilon_y$  is yield strain,  $\sigma_h$  is hydrostatic stress, and  $\sigma_{mises}$  is the von Mises stress. A numerator of Eq. (1) is known as PEEQ Index representing local ductility demand, and  $\sigma_h / \sigma_{mises}$  in the denominator of Eq. (1) is known as triaxiality that causes the reduction in rupture strain of metal (El-Tawil et al., [10]). The value, RI, therefore, is the ratio between the local ductility demand and triaxiality and, in a relative sense, the greater the RI value means the greater fracture potential.

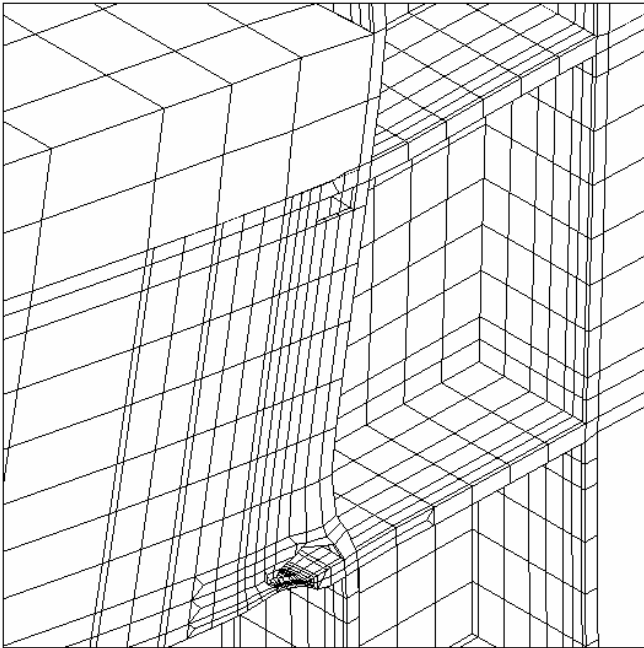
Hancock and Mackenzie [11] introduced the RI concept and showed, at least, 3 types of steel used for their test, the value RI was effective to compare fracture potentials. The RI has been used as an indicator of fracture potential by others (El-Tawil et al., [10]; Mao et al., [12]).

### 4.2 Japanese Connections

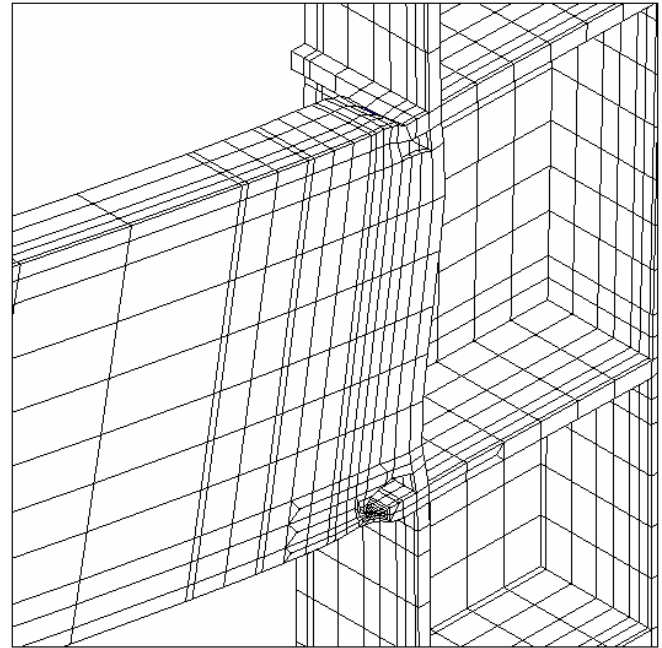
To validate the numerical procedure and model, numerical results are compared with some existing test results. Figures 5 and 6 show that numerical results are close to the test results, which validate the numerical modeling and material properties used in the analysis.

Figure 13 compares the local deformation of S01 and S02 near the column face under almost the same beam tip displacement. It should be noted that these deformed figures are exaggerated 10 times for the clear comparison. In Figure 13(a), the slab and the upper beam flange are deformed relatively small and the deformation is concentrated at the root of beam access hole where possible crack-like defect can be found. The reason of the concentration is that the deformation of the beam upper flange is constrained by the slab as shown from the comparison of the deformation near beam upper flange between Figures 13(a) and 13(b). Most of the beam deformation is contributed by the deformation of the beam lower flange.

In Figure 13(b), on the contrary, the both beam flanges are deformed in compression and tension respectively and the beam web is deformed too. The deformation is distributed over the entire beam cross section at the column face and, consequently, relatively small deformation is occurred at the root of the bottom beam access hole. It should be mentioned that these connections have a strong panel zone so that most of the column panel zone remains in the elastic range even at the ultimate state. In addition, full composite action prevents the relative displacement between the beam and the slab. Therefore, the deformation required to achieve the beam tip displacement is mainly provided by the beam deformation, especially by the beam bottom flange near access hole. The connection with weak panel zone or the partial composite slab may have a different behavior.



**Figure 13(a).** Deformed Shapes (10 times exaggerated), S01 at Beam Tip Disp.= 7.6 cm



**Figure 13(b).** Deformed Shapes (10 times exaggerated), S02 at Beam Tip Disp.= 7.7 cm

Another interesting observation is the deformation of the column flange. A square tube column has two webs at each side but no web at the center where the beam web is connected. Therefore, comparing with the US connection that has only a web at the center, the deformation of the column flange is increased. This will serve as another reason for the fracture occurring near the lower beam flange.

In Figures 14(a) and 14(b), The RI values are plotted at the root of bottom flange access hole where the ductile fracture was initiated. The RI values are plotted against the beam tip displacement and load. The average RI value over the elements near the root of access hole is used.

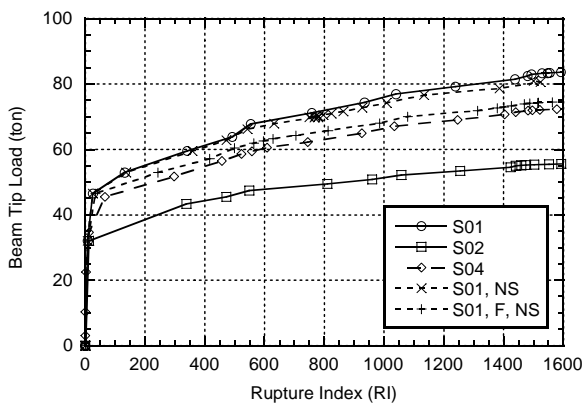


**Figure 14(a).** Rupture Index (RI) vs. Beam Tip Load.

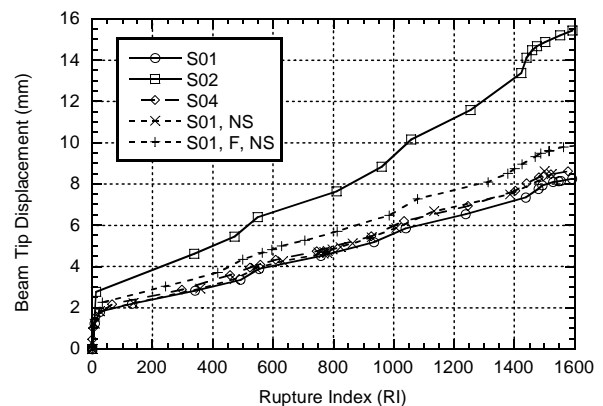


**Figure 14(b).** Rupture Index (RI) vs. Beam Tip Displacement

Figure 14(a) shows that, at the same load level, composite and non-composite connections have different RI values at the root of bottom beam access hole. For example, at the load level of 50 ton, the RI value for S02 has already reached 850, while, for S01 and S04, the values are only 80 and 240, respectively. This means that the composite action increases the strength of the cross section and reduces the fracture potential at the same load level as expected.

In Figure 14(b), at the same beam tip displacement or at the same story drift, the RI value at the root of bottom beam access hole is different. Two composite connections, S01 and S04 have almost twice of RI of S02, non-composite connection, at the same beam tip displacement. For example, at the beam tip displacement of 9 cm, the RI of S02 reaches only 850, but S01 already reaches around 1500. As shown in the deformation figures (Figure 13), this is because, for the composite connection, the deformation near beam is constrained by the slab. Therefore, the deformation required for the beam tip displacement is concentrated near beam bottom flange where the constraint is minimal. For the non-composite connection, the deformation is relatively well distributed over the entire section. This result indicates that, under the same story drift, the composite connection in a steel building has a higher probability of fracture potential than that of the non-composite connection. As mentioned early, practical steel building has floor slabs, the slab that imposes the constraint on the deformation of the connection, should be considered in the design.

Another interesting result is that S01 and S04 have similar values of RI in spite of different slab thickness. In Figure 14(a), these connections have different strengths, and this imply that, if the slab strength is in the practical range, the slab effect is almost the same regardless of slab strength or thickness.

For comparison purpose, two untested composite connections are also modeled. First one is the composite model with no side beams to investigate the effect of the side beams on the constraint (S01, NS in the Figure 14). The other is the composite connection with no side beams and the slab having flute to investigate the effect of the flute on the local buckling of the beam flange (S01, F, NS in the Figure 14). The result shows that no particular effects are found as shown in Figures 14(a) and 14(b) except slight strength difference due to the flute in the slab.

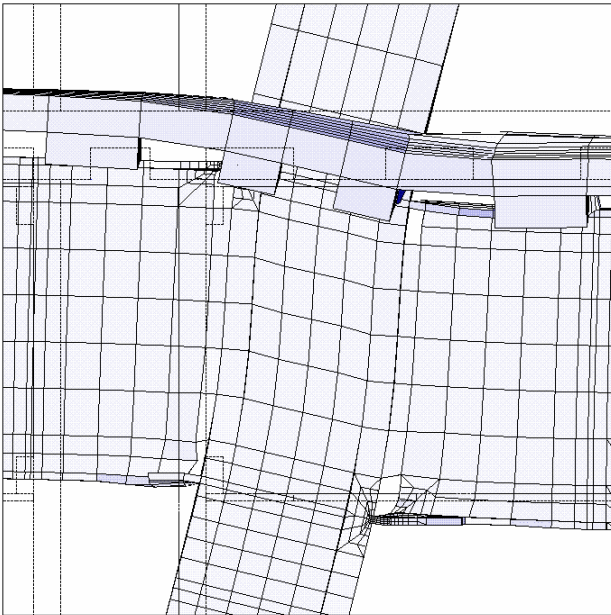
In general, PEEQ index and triaxiality index are given with the RI index as complementary indices. PEEQ index showed almost the same trend as the RI index and triaxiality reached approximately constant value after yielding.

### 4.3 *US Connections*

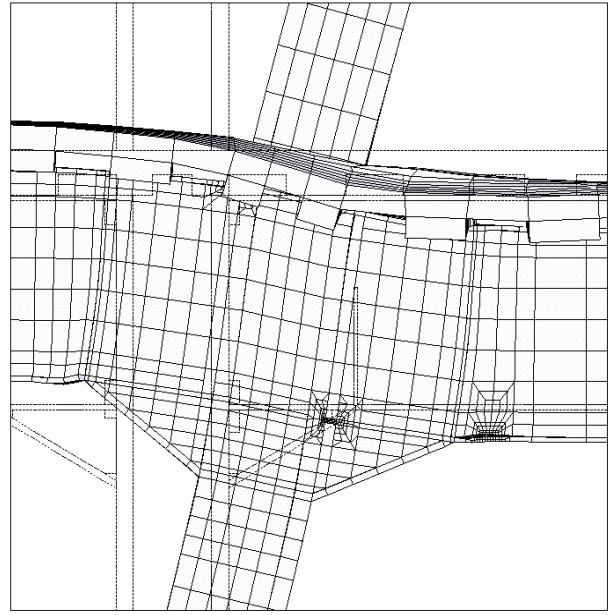
Figures 9, 10, 11 and 12 also show that numerical results are very similar to the test results except that the initial stiffness of the numerical analysis is shafted to the left of the envelope curve. This shift occurs in all models consistently. However, considering that the test results show a sudden change right after loading begins, this shift of the initial stiffness comes from the slip of the test specimens due to the setup.

As shown in the previous section, Figures 15(a) and 15(b) compare the local deformation of RBS and haunch reinforced models respectively under similar column tip displacement. Again, it should be noted that these deformation figures are exaggerated 10 times. Straight dotted line is the un-deformed edges for reference. In Figure 15(a), the deformation is distributed over the connection. The beam flange and access hole are deformed relatively small compared to Japanese connections. In addition, both deformations in the column and panel zone are quite large compared to Japanese connections. The constraint near the beam top flange does not exist. The column tip displacement, the total deformation of the connection, is not contributed by the localized deformation. In Figure 15(b), similarly, beam upper and lower flanges are deformed in compression and tension

respectively and the beam webs, column, and panel zone are also deformed. The deformation is distributed over the beams, column, and panel zone.



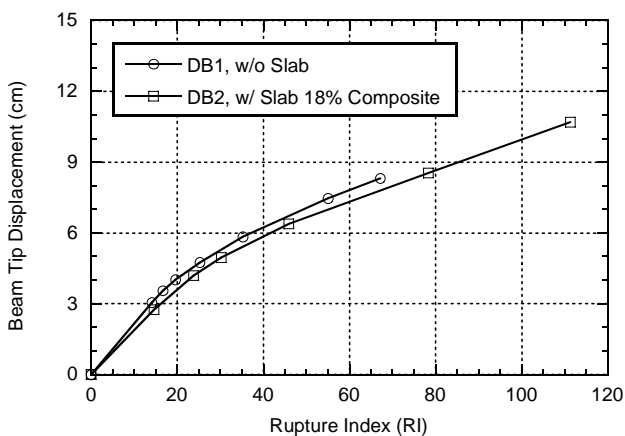
**Figure 15(a).** Deformed Shapes (10 times exaggerated), DB1 at Beam Tip Disp. = 8.6 cm



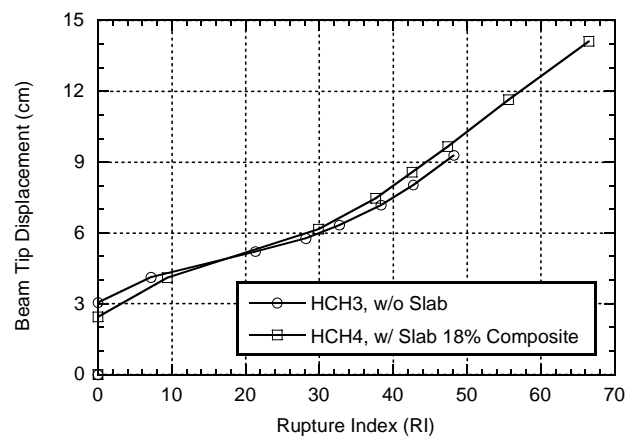
**Figure 15(b).** Deformed Shapes (10 times exaggerated), HCH4 at Beam Tip Disp. = 8.1 cm

Different from the Japanese connections, out of plane deformation of the column flange is evenly distributed due to the column web location. This will serve as another reason for the well distributed deformation for the US connections.

Figures 16(a) and 16(b) compare the RI values of RBS and haunch reinforced models respectively. The RI value is calculated at the column-weld interface for the RBS model and near the end of haunch for the haunch reinforced specimen. The RI values are plotted against the column tip displacement. The maximum displacement in the Figures 16(a) and 16(b) came from the analysis models as shown in Figures 9-12. Again, these RI values may not be exact due to the model simplifications but the relative comparison can help to understand the slab effects.



**Figure 16(a).** Rupture Index (RI) vs. Column Tip Displacement, DB1 and DB2



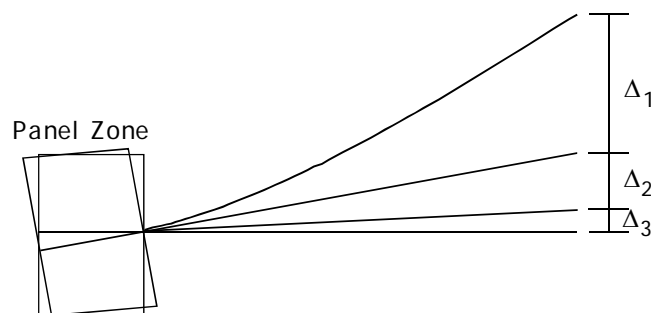
**Figure 16(b).** Rupture Index (RI) vs. Column Tip Displacement, HCH3 and HCH4

Figure 16(a) shows that, at the same displacement level, or at the same story drift, composite and non-composite connections have similar RI values at column-weld interface. In Figure 16(b), at the same beam tip displacement, the RI value near the end of haunch is different slightly, but the absolute value of RI is small. For example, at the column top displacement of 6 cm, the specimens, HCH3 and HCH4, showed the RI values of 44 and 48, respectively. The magnitude of the RI, however, is about 3.0% of that of the Japanese connection. Note that the RI value of Japanese detailed connection is in the range of 1500. Therefore, although there is a some difference in deformation due to the presence of the slab, the slab effect is quite limited as shown in the deformation figures (Figures 15(a) and 15(b)).

## 5. RELATIVE STRENGTH EFFECTS

The deformation capacity of the test specimen is usually measured by the beam or column tip displacements. This tip displacement, however, is not just the displacement from the beam or the column as being implied by its name, but also includes other displacements from the deformation of other components of the connection. In fact, the total displacement consists of three displacements from the deformation of connection components: beams, columns, and panel zone, as shown schematically in Figure 17. Here,  $\Delta_1$ ,  $\Delta_2$ , and  $\Delta_3$  are the beam or column tip displacements due to the deformation of beam, columns, and panel zone, respectively.  $\Delta_1$  and  $\Delta_2$  come from the bending of a beam and a column, and  $\Delta_3$  comes from the shear deformation of the panel zone. The ductility of the connection, therefore, is affected and controlled by the relative strength between the panel zone, the column, and the beam. This is called ‘relative strength effect’ in this paper. The required ductility or tip displacement can be achieved without concentrating the deformation on the beam by controlling the relative strength of the connection components.

Table 5 shows the relative strength of connection components of test specimens. The details of strength calculation of each component are shown in Appendix II. The relative strength is normalized with respect to the beam strength. The Japanese connections, S01 and S02, have a strong panel zone and a strong column. The panel zone and the column should remain elastic when the beam experiences the plastic deformation. The composite connection, S01, has relatively weak panel and column compared to the bare steel connection, S02, due to the full composite action. The US connections have a strong column but weak panel zone, which means a large portion of the ‘tip displacement’ would be contributed by the panel zone deformation. The weak panel zone is permitted by the UBC code (1988). But, according to the reference (Civjan et al., 2000), these connections representing a typical connection prior to 1988, they do not exactly meet the code requirement due to the lack of supplemental web weld.

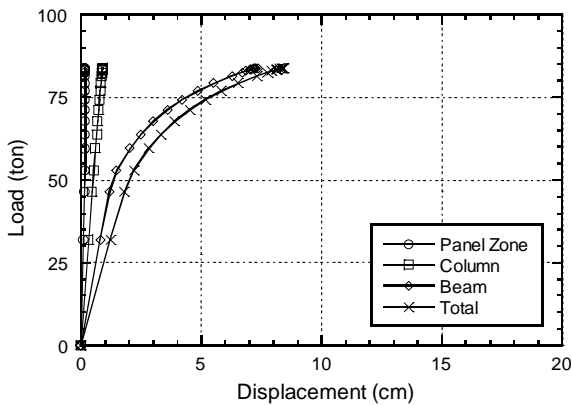
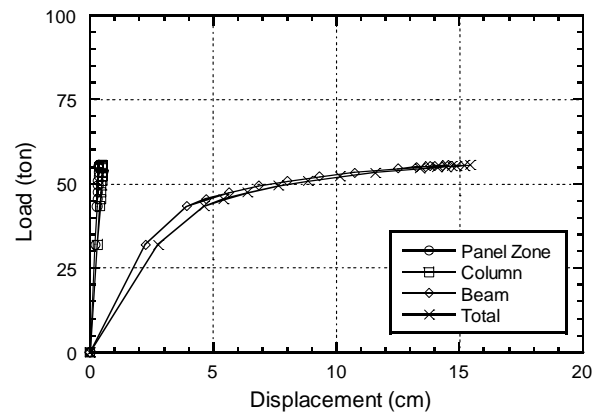


**Figure 17.** Definition of the Displacements from a Beam, a Column, and Panel Zone

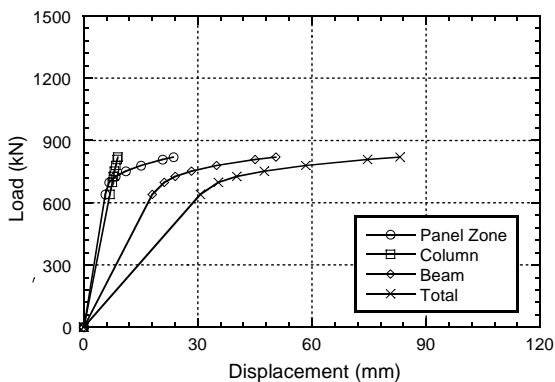
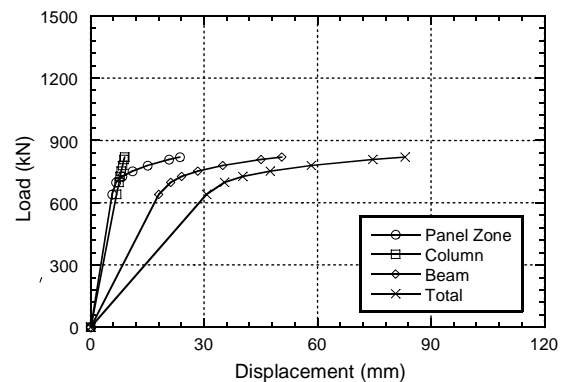
**Table 5.** Relative Strength of Connection Component

| Model<br>(1) | S01<br>(2) | S02<br>(3) | DB1<br>(4) | DB2<br>(5) |
|--------------|------------|------------|------------|------------|
| $P_b/P_b$    | 1          | 1          | 1          | 1          |
| $P_c/P_b$    | 1.96       | 3.77       | 2.13       | 1.75       |
| $P_z/P_b$    | 1.72       | 3.32       | 0.63       | 0.52       |

Figures 18(a) and 18(b) show the relationship between beam tip load and  $\Delta_1$ ,  $\Delta_2$ ,  $\Delta_3$ , and total displacement of S01 and S02. First of all,  $\Delta_3$ , the displacement due to panel zone deformation is very small compared to others and remain in the elastic region. This is because Japanese connections use very thick web and a square column that have two webs as shown in Table 5. The displacement due to column bending ( $\Delta_2$ ) is greater than the panel zone displacement. It is also small compared to the displacement by beam bending. Therefore, most of beam tip displacement is from beam deformation, especially in the inelastic region. For the bare steel connection, S02, most of the tip displacement is from the beam deformation. This result is consistent with the relative strength in Table 5 and previous observation from Figures 13(a) and 13(b).

**Figure 18(a).** Displacement Distribution vs. Loading, S01**Figure 18(b).** Displacement Distribution vs. Loading, S02

The other interesting result is that the displacement by the column bending,  $\Delta_2$ , of the S01, is greater than that of S02, because, as shown in Table 5, the relative strength of beam of S01 is greater than that of S02 due to the composite action. With respect to the distributed deformation, in fact, S01 has slightly better relative strength than that of S02. But the beam deformation of S01 is still very large compared to others. Furthermore, the deformation of the beam top flange is constrained by the slab, which leads to the fracture of the beam bottom flange.

**Figure 19(a).** Displacement Distribution vs. Loading, DB1**Figure 19(b).** Displacement Distribution vs. Loading, DB2

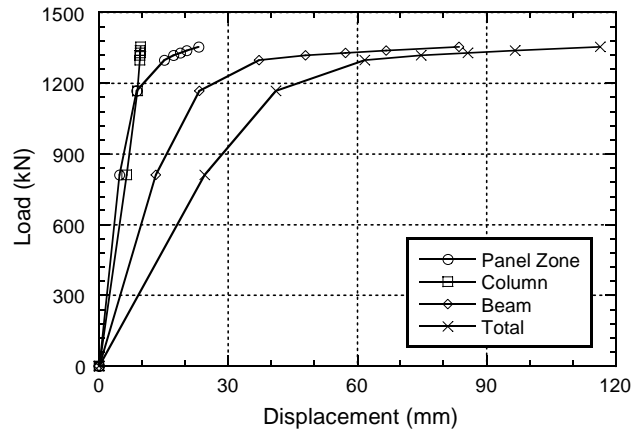
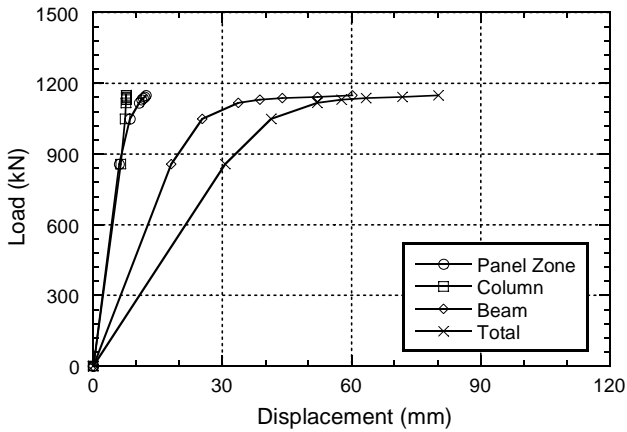


**Figure 20(a).** Displacement Distribution vs. Loading, HCH3 **Figure 20(b).** Displacement Distribution vs. Loading, HCH4

For the US connections, Figures 19(a), 19(b), 20(a), and 20(b) show the displacement distribution of RBS and haunch reinforced connections. First, the displacement distribution is quite different from those of S01 and S02. Displacement by the panel zone deformation is up to about 20% of total displacement at the lower load level and entered into the inelastic range at higher load level. This is expected from the relative strength shown in Table 5, because the strength of the panel zone is smaller than that of the beam, not to mention the column strength. Before panel zone yields, the displacement by the column deformation is almost same with the displacement by panel zone and about 40% of total displacement is contributed by the column and the panel zone. After panel zone yields, the displacement distribution is redistributed due to the changing stiffness of each component. The beam displacement is about 60%, which is a small portion of the total displacement compared to the Japanese connections. The deformation of the US detailed connection is well distributed between beams, a column, and panel zone, as shown in the deformed figures.

By comparing the displacement distribution and relative strength of the Japanese and US connections, the reason why the slab effect is apparently different for different connections can be explained. In the US connections, due to a large panel zone deformation, the beam deformation to meet the desired beam tip displacement is relatively small. Accordingly, the slab effect was not observed. On the contrary, in Japanese connections, all displacements except the beam are suppressed due to the design practice, and consequently, the beam undertook all deformations to meet the beam tip displacement. For a composite connection, this beam deformation is further concentrated at the beam lower flange and access hole due to the confining effect by the slab.

## 6. SUMMARY AND CONCLUSIONS

In this paper, the slab effects on the behavior of composite connections during an earthquake are investigated using numerical analyses based on some existing composite connection tests. Two different connection details are modeled. One is the typical US connection detailing using wide flange sections for both beam and column. Another is the typical Japanese connection details, which are designed to have a square column with a wide flange beam section. Both are designed with strong column-weak beam concept, but the Japanese connection detailing usually has a stronger panel zone and column than that of the US detailing.

Numerical results indicate that the composite slab imposes the constraint on the deformation near the beam top flange. The deformation due to the beam tip displacement is concentrated at the root of beam access hole where the geometry changes abruptly and manufacturing cutting process often leaves crack-like defects. In the test, the brittle fracture at this spot occurred after semi-elliptic shape ductile crack propagated, but energy dissipation and beam tip displacement are far less compared to that of the bare steel connection.

The ultimate strength of the connection is increased with thicker slab, but the fracture potential at the beam access hole is almost the same under the same beam tip displacement. This result implies that the constraint on deformation of the beam section due to the presence of the slab is about the same regardless of slab strength or degree of composite action.

The analyses of the US connections show that the column or beam tip displacement is composed of three displacements from the deformation of the beam, the column, and the panel zone. The magnitude of each displacement depends on the relative strength between connection components. Therefore, even if the beam or column tip displacement is large, the deformation from each member can be small as shown in the US connection cases. This is why the composite connections in the US connection show better ductility than the bare steel connection. The detrimental slab effect is minimized and the beneficial effect is unaffected. It should be mentioned that the deformation in the column and panel zone might cause possible stability problem.

Since numerical analyses show the detrimental slab effects on the ductility of the connection and every practical steel building has composite floor slabs, the detrimental slab effect on possible connection fracture potential should be considered in the connection design. In fact, the slab effect can be minimized by simply adjusting the relative strength between connection components as long as the global stability is assured.

**REFERENCES**

- [1] Federal Emergency Management Agency (FEMA). Recommended seismic design criteria for new steel moment buildings. Rep No FEMA 350. Washington, DC; 2000.
- [2] Nakashima M, Suita K, Morisako K, Maruoka Y. Test of welded beam-column subassemblies I: Global Behavior. *J of Structural Engineering, ASCE* 1998;124(11):1236-1244.
- [3] Joh C, Chen WF. Fracture strength of welded flange-bolted web connections. *J of Structural Engineering, ASCE* 1999;125(5):565-571.
- [4] Research Institute of Industrial Science and Technology (RIST). Earthquake resistance capacity evaluation of steel structural frame considering composite beam effect. Rep No 2000H002. Kyungkido, Korea; 2001.
- [5] Joh C, Chen WF. Seismic Behavior of Steel Moment Connections with Composite Slab. *International Journal of Steel Structures, The Korean Society of Steel Construction* 2001;1(3):175-183.
- [6] ANSYS 5.6 user's manual. ANSYS, Inc. Southpointe 275 Technology Drive, Canonsburg, PA; 1994.
- [7] Civjan SA, Engelhardt MD, Gross JL. Retrofit of pre-Northridge moment-resisting connections. *J of Structural Engineering, ASCE* 2000;126(4):445-452.
- [8] Civjan SA, Engelhardt, MD, Gross JL. Slab effects in SMRF retrofit connection tests. *J of Structural Engineering, ASCE* 2000;127(4):230-237.
- [9] Applied Technology Council (ATC). ATC-24: Guidelines for seismic testing of components of steel structures. Redwood, California; 1992.
- [10] El-Tawil S, Mikesell T, Vidarsson E, Kunnath SK. Strength and ductility of FR welded-bolted connections. Rep No SAC/BD-98/01. SAC Joint Venture, Sacramento, California; 1998.
- [11] Hancock JW, MacKenzie AC. On the mechanisms of ductile failure in high-strength steel subjected to multi-axial stress states. *J Mech Phys Solids* 1976;24:147-169.
- [12] Mao CR, Ricles J, Lu LW, Fisher J. Effect of local details on ductility of welded moment connections. *J of Structural Engineering, ASCE* 2001;127(9):1036-1044.

**APPENDIX: RELATIVE STRENGTH**

The following formulas and symbols are used for the relative strength calculation:

For Exterior Connection Test Setup (El-Tawil et al., 1998)

$$\text{Beam Strength: } P_b = M_{pb} / L_b$$

$$\text{Column Strength: } P_c = 2M_{pc}L_c / (L_b + d_c / 2)(L_c - d_b)$$

$$\text{Panel Zone Strength: } P_z = 0.55F_{yc}d_c t_{wc} \frac{\left[ 1 + 3 \frac{b_{fc} t_{fc}^2}{d_c d_b t_{wc}} \right]}{\left[ \frac{L_b}{0.95d_b} - \frac{L_b + d_c / 2}{L_c} \right]}$$

For Interior Connection Test Setup (load applied from the column top)

$$\text{Column Strength: } P_c = 2M_{pc} / (L_c - d_c)$$

$$\text{Beam Strength: } P_b = 2M_{pb}L_b / (L_c(L_b - d_c))$$

$$\text{Panel Zone Strength: } P_z = 0.55F_{yc}d_c t_{wc} \frac{\left[ 1 + 3 \frac{b_{fc} t_{fc}^2}{d_c d_b t_{wc}} \right]}{2 \left[ \frac{0.5(L_c - d_b)}{0.95d_c} - \frac{0.5L_c}{L_b} \right]}$$

$d$  = Beam or column depth

$t_w$  = Beam or column web thickness

$t_f$  = Beam or column flange thickness

$b_f$  = Beam or column flange width

$P_b$  = Beam or column tip load to make test setup to reach beam strength

$P_c$  = Beam or column tip load to make test setup to reach column strength

$P_z$  = Beam or column tip load to make test setup to reach panel zone strength

$L_b$  = Beam Length

$L_c$  = Column Length

**Subscripts**

$b$  = beam

$c$  = column

